RSC Advances


This is an *Accepted Manuscript*, which has been through the Royal Society of Chemistry peer review process and has been accepted for publication.

*Accepted Manuscripts* are published online shortly after acceptance, before technical editing, formatting and proof reading. Using this free service, authors can make their results available to the community, in citable form, before we publish the edited article. This *Accepted Manuscript* will be replaced by the edited, formatted and paginated article as soon as this is available.

You can find more information about *Accepted Manuscripts* in the Information for Authors.

Please note that technical editing may introduce minor changes to the text and/or graphics, which may alter content. The journal's standard Terms & Conditions and the Ethical guidelines still apply. In no event shall the Royal Society of Chemistry be held responsible for any errors or omissions in this *Accepted Manuscript* or any consequences arising from the use of any information it contains.

ROYAL SOCIETY OF CHEMISTRY

www.rsc.org/advances

# Prelithiated lithium vanadate anode and the mass balancing of its hybrid capacitor

Hao-Yu Wei, Dah-Shyang Tsai,* Chung-Lung Hsieh

Department of Chemical Engineering, National Taiwan University of Science and Technology, 43, Keelung Road, Section 4, Taipei 10607, Taiwan

*Corresponding author
Department of Chemical Engineering, National Taiwan University of Science and Technology, 43, Keelung Road, Section 4, Taipei 10607 Taiwan
E-mail address: dstsai@mail.ntust.edu.tw

**Abstract:** The electrode of sol-gel derived $Li_3VO_4$ (LVO), which exhibits a capacity of 2 moles lithium between 0.01 and 2.0 V (*vs*. $Li/Li^+$), is studied as an anode of the capacitor, matching with the cathode of activated carbon (AC). Before assembling the hybrid capacitor of AC/LVO, $Li_3VO_4$ has been prelithiated. The end potential of prelithiation affects the lithium loading and the resultant cell capacity. The cell, with LVO prelithiation ending at 0.5 V (*vs*. $Li/Li^+$), displays 34% more capacity than the other with LVO ending at 2.0 V (*vs*. $Li/Li^+$). The higher capacity is effected through reducing the electrode potential at 0% state-of-charge of the hybrid capacitor, which also depends on the AC:LVO mass ratio and the specific current. We develop a scheme to estimate the optimal mass ratio for capacitor. The optimal ratio is verified later in galvanostatic charge-discharge experiments, involving four capacitors with the AC:LVO mass ratio 0.5:1, 1:1, 2:1, 3:1. The optimal 2:1 cell demonstrates a capacity of specific energy 49.1 Wh $kg^{-1}$ at 0.05 A $g^{-1}$ and 3.5 V, and 81% retention in the voltage hold test persisting 100 h.

RSC Advances Accepted Manuscript

## Introduction

The capacity of electrochemical capacitor can be upgraded through hybridizing its electrostatic storage mechanism with the battery storage mechanism. The charge transfer reactions of lithium battery are viewed as ideal candidates in complementing the double layer capacitance because of their swift character.[1-4] The high storage capacity of battery electrode may originate from one of three processes, including lithium intercalation of carbonaceous materials,[5,6] insertion reaction of oxide materials,[7,8] alloying reactions with tin or silicon metal.[9-11] Although being usually described as diffusion phenomena, these energetic processes involve bond breaking and formation. Their associated energy barriers make cycling operations featured with considerable resistance,[12] in contrast to small resistance of the double-layer electricity storage.

One of popular hybridizations is the series design of lithium ion hybrid capacitor (LIHC), allowing either the negative or the positive electrode to assume the battery type of charge storage. The LIHCs, with a negative battery electrode, are superior to those with a positive battery electrode in energy and power performance.[13] The success is mainly attributed to a high cell voltage (4.0 V), and an ample supply of electrolyte lithium via lithiated anode.[14-16] Thus, lithiated graphite,[17-20] soft carbons,[21,22] hard carbons[14,16,23,24] have been exploited as the anode. Several ways have been developed to modify the lithiation technique.[16,25,26]

Lithium vanadates could serve as excellent storage material, since they tolerate a wide potential window and exhibit a higher volumetric capacity in comparison with graphite.[27,28] One of the



RSC Advances Accepted Manuscript

candidates is $Li_3VO_4$ (LVO), which crystallizes in an orthorhombic structure, space group $Pmn2_1$, with the lattice parameters *a*=0.6326 nm, *b*=0.5446 nm, *c*=0.4947 nm, isotype with that of $\beta_{II}$ phase $Li_3PO_4$. LVO structure can be viewed as hexagonal close-packed oxygen anions along the [100] direction, balanced by lithium and vanadium cations. Its polyhedron model may be described as corner-shared lithium and vanadium tetrahedra, $LiO_4$ and $VO_4$, stacked alternatively.[29,30] LVO of $\beta_{II}$ phase can accommodate plenty of extra lithium.

Recently, a few research groups have fabricated carbon composite anodes of LVO and studied their battery applications.[30-33] In this work, we synthesize LVO nanoparticles using the citric-acid gel method, and prepare several half cells to investigate the storage capabilities of LVO electrode and activated carbon (AC) electrode. A calculation scheme is devised to estimate the adequate mass balancing with known capacities of the LVO and AC electrodes. Accordingly, the capacitor cells of various mass ratios are assembled to test the prediction and study the energy storage capacity and cycle stability.

## Experimental

### *LVO powder synthesis*

Stoichiometric amounts of $Li_2CO_3$ (0.01575 mole, 5% in excess, Aldrich) and $V_2O_5$ (0.005 mole, ACROS) were weighed and dissolved, along with citric acid (0.06 mole, ACROS), in a beaker that contained 1.0 M ~50 ml nitric acid (Panreac). As the mixture turned into a transparent blue solution,



RSC Advances Accepted Manuscript

the beaker temperature was gradually raised to 70 °C with slow stirring until the solution became a gel. The gel precursor was placed in a furnace and calcined at 400 or 500 °C for 6 h in air. The calcined LVO powder was pulverized with agate mortar and pestle, mixed with Super P carbon black (TIMCAL) in a weight ratio 95:5, and ball milled for 10 h. We labeled the resulting powder as LVO-g, which was a raw material in electrode preparation.

***Electrode preparation***

The dry LVO electrode contained 80 wt. % LVO-g, 10 wt. % Super P, and 10 wt. % PVdF binder (Aldrich). In making the LVO electrode, the above ingredients were blended with a suitable amount of 1-methyl-2-pyrrolidinone (NMP, ACROS) to form the slurry which was subsequently vacuumed to remove trapped bubbles and a fraction of NMP. The slurry was then dispersed on a polished copper current collector of 2 cm in diameter and dried at 80 °C in an oven for 6 h. After drying, the porous active material was pressed to improve contact among solid particles, and its mass was recorded as the weight difference between the dry LVO electrode and the copper disk. The AC electrode was prepared similarly, through dispersing the slurry of activated carbon on top of a polished and etched aluminum thin disk of 2 cm in diameter, then drying and uniaxial pressing. The AC slurry contained 80 wt. % activated carbon (YP-80F, Kuraray Chemical), 10 wt. % Super P, and 10 wt. % PVdF binder in the NMP solvent.

The LVO and the AC electrodes were placed in an argon-filled glove box (GB-100, SunRay Science), and soaked in the electrolyte for ~10 h to wet their porous interfaces thoroughly. The glove



RSC Advances Accepted Manuscript

box was equipped with a load lock vacuum chamber and a gas circulating and purifying system to keep oxygen and water less than 1 ppm. The electrolyte was 1.0 M $LiPF_6$ in ethylene carbonate (EC) and dimethyl carbonate (DMC) solution (50:50 by volume, LB-301, Zhangjiangang Guotai-Huarong).

***Cell assembly and measurement***

The electrodes of LVO and AC were initially tested in half-cell configuration, using a lithium metal foil (2 cm in diameter, 99.9%, Alfa Aesa) as the counter electrode, a small piece of lithium metal as the reference, and the LVO (or AC) electrode as the working electrode. Two layers of 25 μm thick porous polypropylene film (Celgard 2500) were the separator. The half cells were assembled in an electrochemical test cell (SC-Basic, MikroMasch) under argon atmosphere, with a 20-newton spring force clamping the half-cell assembly. Cyclic voltammetries (CV) were performed with a potentiostat (Workstation 5000, Jiehan). In the case of LVO electrode, the CV measurements were carried out in the potential range from 3.0 to 0.01 V (*vs*. $Li/Li^+$) at 0.2 mV $s^{-1}$. For the AC electrode, the CV currents were recorded in three potential ranges of 2.5-3.8, 2.5-4.0, 2.5-4.2 V (*vs*. $Li/Li^+$) with various sweep rates. The lithiation and de-lithiation capacities of LVO were also measured in five galvanostatic charge/discharge cycles at 0.25 C (0.05 A $g^{-1}$) between 2.0 and 0.01 V (*vs*. $Li/Li^+$).

Four capacitor cells were assembled in two-electrode configuration with the AC:LVO mass ratio 0.5:1, 1:1, 2:1, and 3:1 in the MikroMasch cell. The LVO electrode was designated as the negative electrode (anode) and the AC electrode as the positive (cathode). The mass loadings of AC and LVO



RSC Advances Accepted Manuscript

electrode were 0.8 and 1.6 mg $cm^{-2}$ in the 0.5:1 cell, 1.5 and 1.5 mg $cm^{-2}$ in the 1:1 cell, 3.0 and 1.5 mg $cm^{-2}$ in the 2:1 cell, 4.4 and 1.5 mg $cm^{-2}$ in the 3:1 cell. The thickness of AC electrode, after uniaxial pressing, was 13 (0.8 mg $cm^{-2}$), 25 (1.5 mg $cm^{-2}$), 48 (3.0 mg $cm^{-2}$), 72 μm (4.4 mg $cm^{-2}$). The thickness of LVO electrode was 20 μm. The electrolyte and separator of the capacitor cell were the same with those of the half cells described earlier, but the LVO electrode was prelithiated. Prelithiation was performed, using the half-cell configuration of Li/LVO cell, before assembling the AC/LVO cell. The LVO electrode experienced 5 cycles between 2.0 and 0.1 V (*vs*. $Li/Li^+$) at 0.05 A $g^{-1}$ (0.25 C), and the cycling ended at 0.5 V (*vs*. $Li/Li^+$). After prelithiation, the MikroMasch cell was disassembled under argon. The lithium foil, its current collector, and the separator were taken out of the test cell. A new separator and the AC electrode substituted, and the test cell was clamped again under the spring force with the addition of a few drops of electrolyte. For comparison purpose, prelithiation of one LVO electrode was carried out, setting the end potential 2.0 V instead of 0.5 V (*vs*. $Li/Li^+$). This LVO electrode was used in assembling a capacitor with the AC:LVO mass ratio 2:1.

Galvanostatic tests of the four AC/LVO capacitors were operated with the anode potential being monitored during cycling in the voltage window ($\Delta U$) 3.0 or 3.5 V, using a multichannel potentiostat (1470E, Solartron). With the knowledge of cell voltage and anode potential, the cathode potential was calculated. These electrode potential data were taken after several cycles at the specific current in the preset voltage window, and were analyzed to understand the roles of electrode during charge/discharge.



RSC Advances Accepted Manuscript

***Material characterization***

Crystalline phases of calcined LVO powder were analyzed with an X-ray diffractometer (D2 Phaser, Bruker), equipped with the CuKα radiation source and nickel filter. The crystallite size was estimated with the Scherrer formula, $0.9\lambda/B\cos\theta$, in which $\lambda$ was the wavelength (0.15406 nm), $B$ was the full width at half maximum (FWHM) of the diffraction line at Bragg angle $\theta$. Nitrogen adsorption and desorption isotherms of YP-80F were measured with a surface-area and pore-size analyzer (ASAP2020, ASAP2010, Micrometritics).

**Results and discussion**

***LVO nanocrystals and the electrodes***

The diffraction pattern of 400 °C fired $Li_3VO_4$ powder is plotted in Figure 1. These diffraction lines are indexed on an orthorhombic unit cell with the fitted parameters $a$=0.6316 nm, $b$=0.5441 nm, $c$=0.4945 nm. The crystallite size of 400 °C $Li_3VO_4$ powder is estimated 47 nm, using the FWHM value of its strongest diffraction line (101), at $2\theta$=22.88°. If the firing temperature is raised to 500 °C, the pattern looks similar, but the diffraction peaks sharpen and the crystallite size grows to 52 nm. In this work, the 400 °C powder is used exclusively in the measurements.

Figure 2 presents the surface area analysis result of YP-80F carbon and cyclic voltammograms of the AC electrode. The nitrogen adsorption and desorption isotherms for YP-80F are shown in Figure 2a. When the relative pressure ($P/P_0$) increases from $1.6\times10^{-6}$ to 0.3, the cumulative adsorbed gas



RSC Advances Accepted Manuscript

volume reaches 690 $cm^3$ $g^{-1}$, the adsorption has completed 87.7% of its total adsorption volume 787 $cm^3$ $g^{-1}$. Clearly, YP-80F is a microporous AC with a small fraction of mesopores, showing the type-I isotherm. The hysteresis between relative pressure 0.4 and 1.0, indicates the mesopores are featured with ink-bottle pore shape. The BET plot, as shown in the inset, reports the adsorbed quantity of one monolayer, resulting in a surface area of 2344 $m^2$ $g^{-1}$. This value approximates the upper limit of the quoted surface area of the manufacturer, 1900 – 2300 $m^2$ $g^{-1}$.

Figure 2b shows voltammograms of the AC electrode with various sweep rates in the potential range between 2.5 and 4.0 V (*vs*. $Li/Li^+$). These rectangular-shaped voltammograms display distinctive features of double layer capacitance. Based on these CV results, we calculate the capacitance values according to the following equation, $Q_{CV} / 2(m_{AC}\Delta V)$, where $Q_{CV}$ is the sum of anodic and cathodic charge, $m_{AC}$ is the mass of activated carbon, $\Delta V$ is the scanned potential range. Figure 2c summarizes these capacitance values in three scanned potential ranges, showing the maximum capacitance 74 - 160 F $g^{-1}$ at 1.0 mV $s^{-1}$. In general, the capacitance of AC electrode decreases as the sweep rate increases, and increases with a wider scan window.

The capacity of LVO electrode is reported in Figure 3a, which shows lithiation and delithiation curves of LVO between 0.01 and 2.0 V (*vs*. $Li/Li^+$) at 50 mA $g^{-1}$. Ignoring the first lithiation trace, the other four lithiation curves demonstrate a slightly decreasing storage capacity, ~400 mAh $g^{-1}$, which is similar to the capacity reported by Ni and coworkers,[30] somewhat higher than that of the CNT/LVO composite,[31] but less than the values reported on the LVO/graphene composite,[32] and the



RSC Advances Accepted Manuscript

carbon coated LVO.[33] The capacity 400 mAh $g^{-1}$ approximately equals to two moles of lithium insertion, knowing that one mole lithium insertion corresponds to 197.4 mAh $g^{-1}$ for $Li_3VO_4$. The delithiation capacity also decreases with increasing cycle number, from 400 mAh $g^{-1}$ to 348 mAh $g^{-1}$. The potentials of lithiation and delithiation plateaus are marked in Figure 3a.

Figure 3b presents the first five CV cycles of LVO electrode between 0.01 and 3.0 V (*vs*. $Li/Li^+$). Consistent with the earlier result, the first cycle is distinctively different from the other four in the cathodic scans. Figure 3b shows the two cathodic peaks at 0.5 and 0.79 V of the first cycle shift to 0.55 and 0.90 V (*vs*. $Li/Li^+$) in the latter cycles. And the two anodic peaks at 1.3 and 2.6 V (*vs*. $Li/Li^+$) exhibit no shifting in the anodic scans. Shifting in the cathodic peak positions may result from solid electrolyte interface (SEI) formation during lithiation.

***LVO prelithiation***

When matching with an AC electrode, the extra lithium loading of LVO electrode decreases the potential value at 0% state-of-charge ($U_{0\%SOC}$) and draws more capacity out of the matching electrode. $U_{0\%SOC}$ is defined as the potential value of positive and negative electrodes begin to split during capacitor charging, as well as when they merge at the end of discharging during steady operation. We contrast two cells of different prelithiation levels in Figure 4. The two cells, with the same AC:LVO ratio 2:1, are operated in $\Delta U$=3.5 V and 50 mA $g^{-1}$. Figure 4a shows that when the cell is equipped with a prelithiated LVO electrode ending at 2.0 V, $U_{0\%SOC}$ is 1.86 V (*vs*. $Li/Li^+$), higher than 1.65 V (*vs*. $Li/Li^+$) of the cell equipped with a LVO electrode ending at 0.5 V, Figure 4b.



RSC Advances Accepted Manuscript

Referring to Figure 3, we understand the 0.5 V LVO electrode is richer in lithium than the 2.0 V LVO electrode, that is, 1.42 mole more lithium per gram of LVO. This cell, equipped with a prelithiated anode ending at 0.5 V, begins charging at 1.65 V (*vs*. $Li/Li^+$), its negative electrode potential is situated at a superior location in exploiting the LVO capacity, since this part of lithiation curve is flatter compared with the location of 1.86 V (*vs*. $Li/Li^+$). A flatter potential curve means the negative electrode utilizes a smaller fraction of voltage window, consequently the positive AC electrode takes up a larger share of 3.5 V, and resulting in a higher cell capacity. Figure 4b shows that discharge of this cell, with $U_{0\%SOC}$ 1.65 V, persists 2824 s at 50 mA $g^{-1}$, longer than that of the cell with $U_{0\%SOC}$ 1.86 V, which lasts 2097 s. The cell with $U_{0\%SOC}$ 1.65 V demonstrates a 34% increase in capacity.

The electrode potentials of the two 2:1 cells provide more details on why their capacities differ. Figure 4a shows an initial potential drop, 0.47 V (marked), in charging the negative electrode, larger than 0.26 V of Figure 4b. This potential drop is undesirable or even wasteful, because only a very small quantity of electricity is stored during this sudden potential drop. In other words, the cell, with a prelithiated anode ending at 0.5 V, wastes a smaller fraction of voltage window, compared with the cell with a prelithiated anode ending at 2.0 V. With the same amount of AC loading, Figure 4b shows a potential difference 2.55 V on the positive electrode, less than 2.25 V of Figure 4a. It means more charge accumulated at the positive AC electrode in Figure 4b, which is attributed to the lower $U_{0\%SOC}$ position due to extra loaded lithium at the anode. Hence, all the capacitors, discussed later, implement the prelithiated LVO electrode that ended at 0.5 V (*vs*. $Li/Li^+$).



RSC Advances Accepted Manuscript

***AC:LVO mass ratio***

Knowing the individual electrode capacities, we may calculate the mass ratio that the cell capacity reaches its maximum. The first step is to convert the LVO capacity in mAh $g^{-1}$ into potential dependent capacitance F $g^{-1}$, as illustrated in Figure 5a. The negative electrode of capacitor is assumed to perform just like the 200 mA $g^{-1}$ lithiation curve of the fifth cycle between 0.5 and 2.0 V (*vs*. $Li/Li^+$), as shown in the inset of Figure 5a. The negative electrode capacitance ($C_-$) is calculated using Eq. (1), when the LVO potential descends from 2.0 V ($U_0$) to a minimum potential ($U_{min}$).

$$C_- = \frac{Q_-}{\Delta U_-} = \frac{I \times \Delta t}{U_0 - U_{min}} \quad , \qquad (1)$$

in which $Q_-$ is the accumulated charge when lithiation occurs between $U_0$ and $U_{min.}$ $\Delta U_-$ denotes the potential difference ($U_0$-$U_{min}$), $I$ is the specific current, and $\Delta t$ is the time span. When $\Delta U_-$ is less than 0.6 V, Figure 5a indicates that the capacitance $C_-$ increases slowly with increasing $\Delta U_-$. When $\Delta U_-$ is raised over 0.6 V, the capacitance $C_-$ increases sharply, since $U_{min}$ enters the potential region of ample lithium storage. We further assume the positive electrode of capacitor behaves just like the 5 mV $s^{-1}$ CV result of AC, because the anodic current of 5 mV $s^{-1}$ CV is near 200 mA $g^{-1}$, which is the specific current flowing through the negative electrode. The capacitance of AC positive electrode is denoted as $C_+$, 70.2 F $g^{-1}$, marked in Figure 5b. With the known $C_+$ and $C_-$, we calculate the cell capacitance of AC/LVO capacitor, $C_{LIHC}$, in various mass ratios, $m_+$:$m_-$, using the following equation.

$$C_{LIHC} = \frac{C_- m_- C_+ m_+}{(C_- m_- + C_+ m_+)(m_- + m_+)} \qquad (2)$$

Figure 5c presents the predicted values of cell capacitance, according to Eq. (2). Three curves of



RSC Advances Accepted Manuscript

$C_{LIHC}$, assuming that $\Delta U_{-}$ equals 1.0, 1.25, or 1.5 V, climax at the $m_{+}$:$m_{-}$ ratio 2.0:1, 2.2:1, 2.4:1; individually. Evidently the predicted $m_{+}$:$m_{-}$ ratio is not a precise value, because this ratio varies with $\Delta U_{-}$, which varies with the specific current and voltage window of capacitor. Still it is reasonable to conclude the maximum cell capacity is located near the 2:1 ratio.

We assemble four capacitors with the AC:LVO ratio, 0.5:1, 1:1, 2:1, 3:1, to examine the calculation result. The voltage window is preset to be 3.5 V. The specific cell capacities, listed in Table 1, are 27.4 (0.5:1), 36.2 (1:1), 39.2 (2:1), and 26.8 (3:1) mAh $g^{-1}$, confirming 2:1 is the optimal mass ratio. Although the optimal ratio is correct, we note the dependence of cell capacity on the mass ratio is quite different from that of Figure 5c. The experimental capacity of 3:1 cell is obviously too low. According to Figure 5c, the capacity of the 3:1 cell is expected at least 40% higher than that of the 0.5:1 cell. Our assembled 0.5:1 and 3:1 cells have a nearly equal capacity. The cell capacities of $\Delta U$=3.0 V, not listed in Table 1, display the same trend.

Table 1 indicates the $U_{0\%SOC}$ value is not a constant, this potential value is strongly influenced by the AC:LVO mass ratio. Operated at 50 mA $g^{-1}$, $U_{0\%SOC}$ is recorded 1.34 V of the 0.5:1 cell, rises to 1.38 V for the 1:1 cell, further increases to 1.65 V for the 2:1 cell, and 1.95 V (*vs*. $Li/Li^{+}$) of the 3:1 cell. Moreover, the potential is also affected by the operating current for a particular AC:LVO ratio. Table 2 indicates, for the 2:1 cell, the $U_{0\%SOC}$ value increases with increasing specific current; 1.65 V at 50 mA $g^{-1}$ and 2.04 V (*vs*. $Li/Li^{+}$) at 1.0 A $g^{-1}$. For the 1:1 cell, the rising trend is less steep, varying from 1.38 V at 50 mA $g^{-1}$ to 1.54 V (*vs*. $Li/Li^{+}$) at 1.0 A $g^{-1}$.



RSC Advances Accepted Manuscript

Figure 6 shows how the $U_{0\%SOC}$ position affects the voltage partition of a capacitor with $\Delta U$= 3.5 V and $I$= 50 mA $g^{-1}$. We denote the difference between $U_{0\%SOC}$ and the maximum positive potential as $\Delta U_+$, and the difference between $U_{0\%SOC}$ and the minimum negative potential as $\Delta U_-$. The sum of $\Delta U_+$ and $\Delta U_-$ equals the voltage window. For the 0.5:1 cell, Figure 6a, the $U_{0\%SOC}$ value is relatively low and the negative electrode exploits the most capacitive region of prelithiated LVO. Therefore, $\Delta U_-$ is small, 0.5 V, $\Delta U_+$ occupies a major fraction of the voltage window, $\Delta U_+$=3.0 V. Evidently, the capacity of positive electrode is restricting the cell capacity, since the positive electrode capacity is much less than that of the in-series negative electrode. When the AC:LVO ratio is raised to 1:1, $\Delta U_+$ decreases to 2.70 V and $\Delta U_-$ increases to 0.80 V, Figure 6b. The cell capacity is improved. The AC capacity is still the limiting factor of cell capacity. Meanwhile, we note a subtle difference between Figure 6b and 6a; a small drop in negative potential 0.06 V emerges in Figure 6b, which cannot be found in 6a. Electrode potentials of the 2:1 cell have been plotted in Figure 4b, showing a larger drop 0.26 V in the negative potential trace. Further increasing the AC:LVO ratio to 3:1, the drop increases to 0.55 V, and the voltage partition becomes $\Delta U_+$ 2.1 V and $\Delta U_-$ 1.40 V. The above statement emphasizes again that the potential drop at the beginning of charging is a waste of the voltage window. Hence, the increasing potential drop with respect to increasing mass ratio means that the LVO electrode becomes less capacitive with increasing mass ratio. Consequently, a rising $U_{0\%SOC}$ value produces a more rapid decline than the model predicts in cell capacity with respect to the increasing mass ratio.



RSC Advances Accepted Manuscript

***Energy, power, and stability***

Figure 7 presents the energy and power capacities of the 2:1 cell, operated in two voltage windows, 3.0 and 3.5 V. Values of the specific energy ($E_{cell}$) and specific power ($P_{cell}$) are calculated with the following equations.

$$E_{cell} = I \int_{t_i}^{t_f} U dt \qquad (3) \quad ;$$

$$P_{cell} = \frac{E_{cell}}{(t_f - t_i)} \qquad (4) \quad ;$$

where $I$ is the specific current based on the combined mass of the two electrodes; $t_i$, $t_f$ are the start time and the end time of cell discharge; $U$ is the cell voltage. As expected, a wider voltage window stores more energy. The specific energy of Figure 7b is generally higher than that of Figure 7a at the same specific current. For example, at 50 mA $g^{-1}$, the specific cell energy reaches 49.1 Wh $kg^{-1}$ with $\Delta U$=3.5 V, while the specific energy is 29.3 Wh $kg^{-1}$ with $\Delta U$= 3.0 V. Because of the sluggish LVO electrode, the power of hybrid capacitor is often considered insufficient. One way to raise the power performance is lifting the cutoff voltage. When the cutoff voltage is raised to 1.0 V, instead of 0.01 V (practical zero), energy performance is traded for power performance. Figure 7b shows that the specific energy and power are 49.1 Wh $kg^{-1}$ and 72.5 W $kg^{-1}$ with the cutoff voltage 0.01 V, and turning into 40.9 Wh $kg^{-1}$ and 103.1 W $kg^{-1}$ with the cutoff voltage 1.0 V. Further lifting the cutoff voltage to 2.0 V, the increase in power costs too much energy reduction, the specific energy and power become 24.5 Wh $kg^{-1}$ and 129.7 W $kg^{-1}$ at 50 mA $g^{-1}$. Similar trade-off is shown in Figure 7a.

Figure 8 shows the stability of this AC/LVO capacitor with a 2:1 mass ratio. We employ the



RSC Advances Accepted Manuscript

voltage hold test which has been described more demanding than the uninterrupted cycling test.[34,35] The cell voltage of the 2:1 cell is first held at 3.5 V for 4 h, then the cell charges and discharges at 200 mA $g^{-1}$ in $\Delta U$=3.5 V. After 3 galvanostatic cycles, the cell voltage is held at 3.5 V for another 4 h. The procedure of holding at 3.5 V and cycling 3 times is repeated until the hold time totals up to 100 h. Figure 8 shows the values of capacitance and coulombic efficiency, measured in the third cycle every 4 h. Initially, the cell capacitance is 28.8 F $g^{-1}$, gradually decreases with the hold time, down to 23.3 F $g^{-1}$ at the end of 100 h, which is 81% retention in capacity. The coulombic efficiency maintains at 97-95% throughout the period. This stability performance is similar to that of the lithium ion capacitor of prelithiated graphite, which shows 83% capacity retention after 100 h voltage hold.[36] If the 2:1 cell of AC/LVO undergoes the voltage hold test in a wider window, 3.8 V, the cell capacitance decays much faster. After 100 h, the capacity loss is 37%. Hence we conclude 3.5 V is a suitable voltage window for the 2:1 cell, taking lifetime into consideration.

## Conclusions

The LVO powder of nanometer size has been synthesized at 400 °C and investigated as the active material for hybrid capacitor. Prelithiation of the LVO electrode has been conducted and ended at 0.5 V to load a sufficient amount of lithium ion in the LVO host. The preloaded lithium augments the storage capacity of LVO/AC by 34%. The optimal matching quantity of AC is approximately twice the amount of LVO. Unfortunately, the calculation scheme does not yield a more precise value



RSC Advances Accepted Manuscript

because the $U_{0\%SOC}$ value shifts with the AC:LVO ratio and the specific current considerably. The 2:1 cell shows a sufficient stability in $\Delta U$= 3.5 V. It demonstrates large capacities at low specific currents, and resumes high power attributes of a capacitor at high specific currents.

**Acknowledgements**

This work is financially supported by Ministry of Science and Technology of Taiwan through the project MOST-103-2221-E-011-153-MY3. The miscellaneous fees are paid through one of Top University Projects 104H45140 *via* National Taiwan University of Science and Technology.

RSC Advances Accepted Manuscript

Table 1 Cell capacities, $U_{0\%SOC}$ (*vs*. Li/Li$^+$), and $\Delta U_+$ and $\Delta U$- of the cells with four AC:LVO mass ratios, operated at 50 mA g$^{-1}$ in the voltage window $\Delta U$=3.5 V.

| AC:LVO | 0.5:1 | 1:1 | 2:1 | 3:1 |
|---|---|---|---|---|
| Cell capacity (mAh g$^{-1}$) | 27.4 | 36.2 | 39.2 | 26.8 |
| $U_{0\%SOC}$ (V) | 1.34 | 1.38 | 1.65 | 1.95 |
| $\Delta U_+$ (V) | 3.00 | 2.70 | 2.55 | 2.10 |
| $\Delta U$- (V) | 0.50 | 0.80 | 0.95 | 1.40 |

RSC Advances Accepted Manuscript

Table 2 Variations of $U_{0\%SOC}$ (*vs*. Li/Li$^+$) with respect to specific current for two capacitors with the AC:LVO ratio, 2:1 and 1:1. Both cells are operated in $\Delta U$=3.5 V. The mass loadings are 1.5 (AC) and 1.5 (LVO) mg cm$^{-2}$ in the 1:1 cell, 3.0 (AC) and 1.5 (LVO) mg cm$^{-2}$ in the 2:1 cell. The electrode thickness is 25 (1.5 mg cm$^{-2}$), 48 (3.0 mg cm$^{-2}$) μm for the AC electrode, and 20 μm for the LVO electrode.

| Current (mA g$^{-1}$) | 50 | 70 | 100 | 200 | 500 | 1000 |
|---|---|---|---|---|---|---|
| $U_{0\%SOC}$ (V) for 2:1 | 1.65 | 1.68 | 1.72 | 1.79 | 1.92 | 2.04 |
| $U_{0\%SOC}$ (V) for 1:1 | 1.38 | 1.38 | 1.38 | 1.39 | 1.45 | 1.54 |

RSC Advances Accepted Manuscript

**References**

1. W. Cao, J. Zheng, D. Adams, T. Doung and J.P. Zheng, *J. Electrochem. Soc.*, 2014, **161**, A2087-A2092.

2. D. Cericola and R. Kotz, *Electrochim. Acta*, 2012, **71**, 1-17.

3. N. Omar, M. Daowd, O. Hegazy, M. Al Sakka, Th. Coosemans, P. Van den Bossche and J. Van Mierlo, *Electrochim. Acta*, 2012, **86**, 305-315.

4. P.H. Smith, T.N. Tran, T.L. Jiang and J. Chung, *J. Power Sources*, 2013, **243**, 982-992.

5. C. Decaux, G. Lota, E. Raymundo-Pinero, E. Frackowiak and F. Beguin, *Electrochim. Acta*, 2012, **86**, 282-286.

6. M.S. Balogun, W. Qiu, W. Wang, P. Fang, X. Lu and Y. Tong, *J. Mater. Chem. A*, 2015, **3**, 1364-1387.

7. V. Aravindan, J. Gnanaraj, Y.S. Lee and S. Madhavi, *Chem. Rev.*, 2014, **114**, 11619-11635.

8. K. Naoi, *Fuel Cells*, 2010, **10**, 825-833.

9. J. Graetz, C.C. Ahn, R. Yazami and B. Fultz, *Electrochem. Solid-State Lett.*, 2003, **6**, A194-A197.

10. M.T. McDowell, S.W. Lee, W.D. Nix and Y. Cui, *Adv. Mater.*, 2013, **25**, 4966-4985.

11. X. Li , X. Meng , J. Liu , D. Geng , Y. Zhang, M.N. Banis , Y. Li , J. Yang , R. Li , X. Sun, M. Cai and M.W. Verbrugge, *Adv. Funct. Mater.*, 2012, **22**, 1647-1654.

12. M.D. Levi and D. Aurbach, *J. Phys. Chem. B*, 1997, **101**, 4641-4647.

13. A. Brandt and A. Balducci, *Electrochim. Acta*, 2013, **108**, 219-225.



RSC Advances Accepted Manuscript

14. W.J. Cao and J.P. Zheng, *J. Electrochem. Soc.*, 2013, **160**, A1572-A1576.

15. J.P. Zheng, *J. Electrochem. Soc.*, 2009, **156**, A500-A505.

16. W.J. Cao and J.P. Zheng, *J. Power Sources*, 2012, **213**, 180-185.

17. S.R. Sivakkumar and A.G. Pandolfo, *Electrochim. Acta*, 2012, **65**, 280-287.

18. J.H. Lee, W.H. Shin, S.Y. Lim, B.G. Kim and J.W. Choi, *Mater. Renew. Sustain. Energy*, 2014, **3**, 22 (8 pages).

19. V. Khomenko, E. Raymundo-Pinero and F. Beguin, *J. Power Sources*, 2008, **177**, 643-651.

20. T. Aida, K. Yamada and M. Morita, *Electrochem. Solid-State Lett.*, 2006, **9**, A534-A536.

21. M. Schroeder, M. Winter, S. Passerini and A. Balducci, *J. Power Sources*, 2013, **238**, 388-394.

22. M. Schroeder, M.Winter, S. Passerini and A. Balducci, *J. Electrochem. Soc.*, 2012, **159**, A1240-A1245.

23. X. Sun, X. Zhang, H. Zhang, N. Xu, K. Wang and Y. Ma, *J. Power Sources*, 2014, **270**, 318-325.

24. Y.G. Lim, J.W. Park, M.S. Park, D. Byun, J.S. Yu, Y.N. Jo and Y.J. Kim, *Bull. Korean Chem. Soc.*, 2015, **36**, 150-155.

25. J.P. Zheng, *J. Electrochem. Soc.*, 2009, **156**, A500-A505.

26. M.S. Park, Y.G. Lim, J.H. Kim, Y.J. Kim, J. Cho and J.S. Kim, *Adv. Energy Mater.*, 2011, **1**, 1002-1006.

27. C.J. Peng, D.S. Tsai, C. Chang and H.Y. Wei, *J. Power Sources*, 2015, **274**, 15-21.

28. N. Bockenfeld and A. Balducci, *J. Power Sources*, 2013, **235**, 265-273.



RSC Advances Accepted Manuscript

29. R.D. Shannon and C. Calvo, *J. Solid State Chem.*, 1973, **6**, 538-549.

30. S. Ni, X. Lv, J. Ma, X. Yang and L. Zhang, *J. Power Sources*, 2014, **248**, 122-129.

31. Q. Li, J. Sheng, Q. Wei, Q. An, X. Wei, P. Zhang and L. Mai, *Nanoscale*, 2014, **6**, 11072-11077.

32. Z. Jian, M. Zheng, Y. Liang, X. Zhang, S. Gheytani, Y. Lan, Y. Shi and Y. Yao, *Chem. Commun.*, 2015, **51**, 229-231.

33. Z. Liang, Z. Lin, Y. Zhao, Y. Dong, Q. Kuang, X. Lin, X. Liu and D. Yan, *J. Power Sources*, 2015, **274**, 345-354.

34. D. Weingarth, A. Foelske-Schmitz and R. Kotz, *J. Power Sources*, 2013, **225**, 84-88.

35. D. Weingarth, A. Foelske-Schmitz, A. Wokaun and R. Kotz, *Electrochim. Acta*, 2013, **103**, 118-224.

36. S. Kumgai, T. Ishikawa and N. Sawa, *J. Energy Storage*, 2015, **2**, 1-7.

RSC Advances Accepted Manuscript

**Figures and captions**

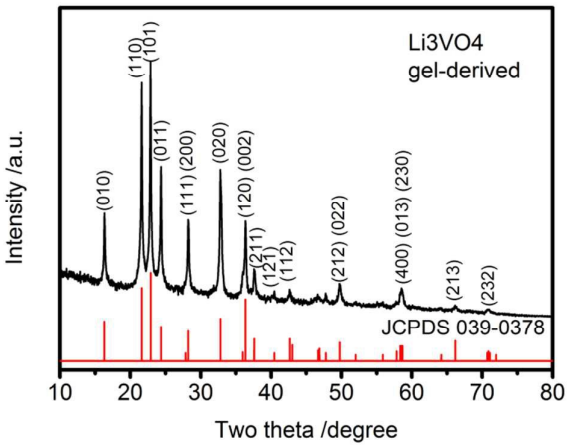


**Figure 1** X-ray diffraction result of $Li_3VO_4$ nanocrystals. The pulverized LVO powder was calcined at 400 °C for 6 h, and its diffraction pattern contrasts with the orthorhombic $Li_3VO_4$ standard file JCPDS 039-0378.

RSC Advances Accepted Manuscript

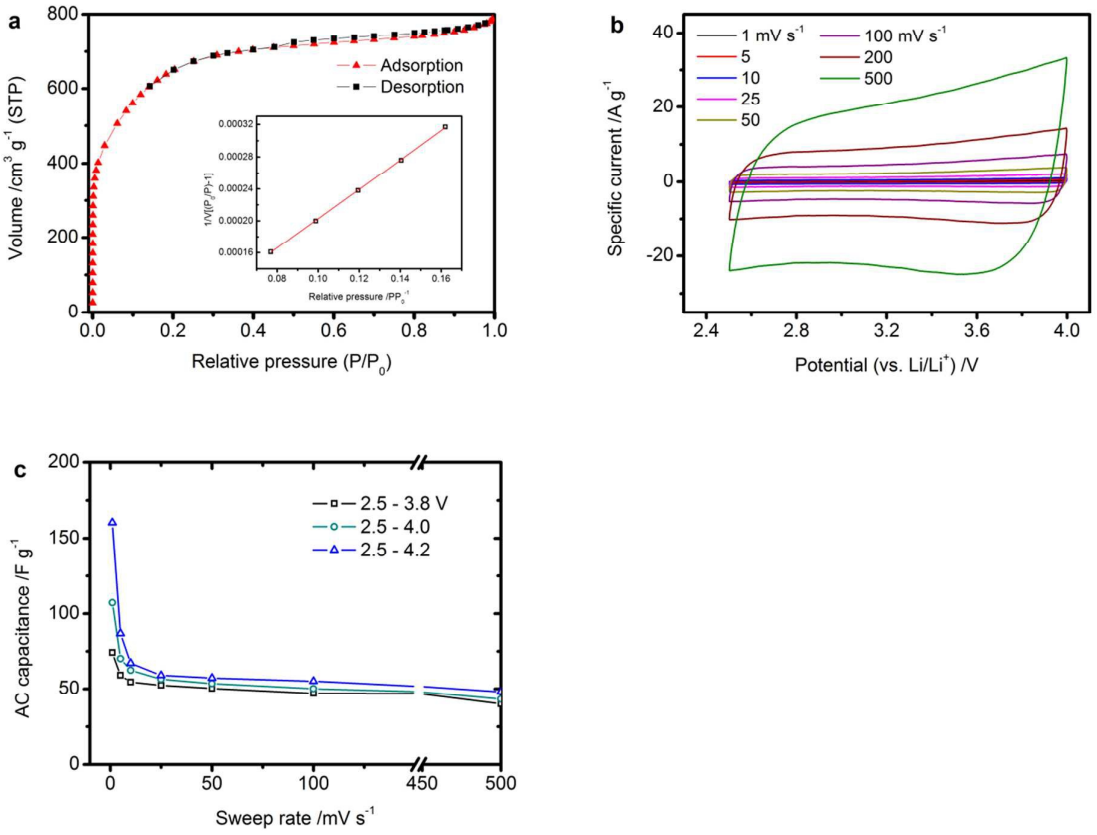


**Figure 2** Surface area analysis of AC and double layer capacitance of the AC electrode. (a) 77 K nitrogen isotherms of YP-80F AC and the inset of BET plot based on adsorption isotherm. (b) AC voltammograms measured in a Li/AC half cell at 1, 5, 10, 25, 50, 100, 200, 500 mV $s^{-1}$. (c) The AC capacitance values at various sweep rates in 2.5-3.8 V, 2.5-4.0 V, 2.5-4.2 V (*vs*. Li/$Li^+$).

RSC Advances Accepted Manuscript

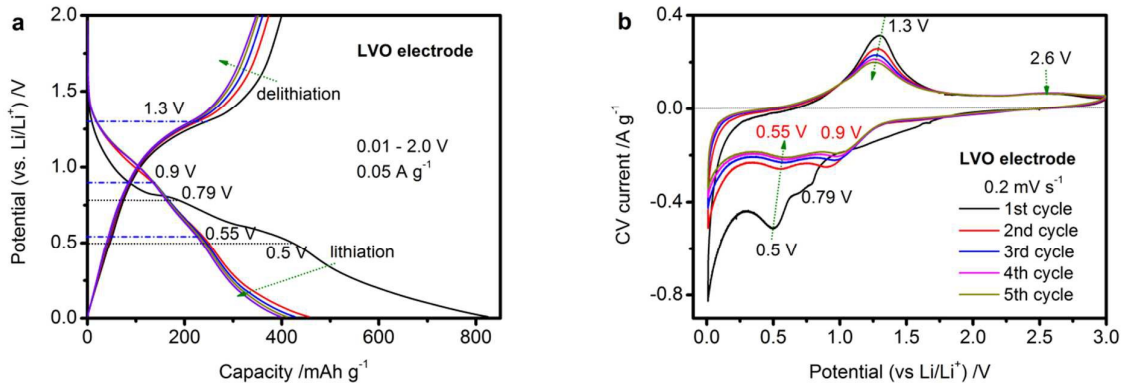


**Figure 3** Electrochemical characterization of the LVO electrode. (a) Five cycles of lithiation and delithiation at 50 mA $g^{-1}$ (0.25 C) between 2.0 and 0.01 V (*vs*. $Li/Li^+$) with the plateau potentials marked. (b) Five CV cycles of the LVO electrode at 0.2 mV $s^{-1}$ between 3.0 and 0.01 V (*vs*. $Li/Li^+$), noting the peak shifts.

RSC Advances Accepted Manuscript

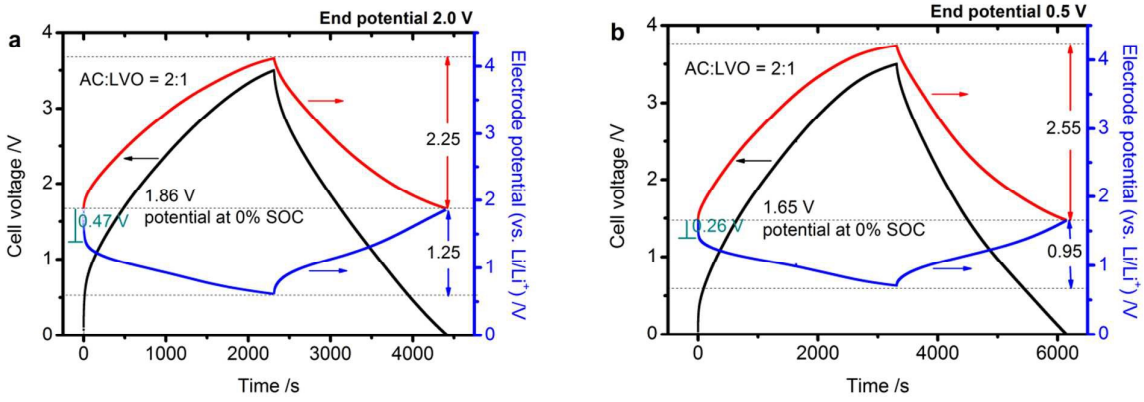


**Figure 4** Effects of extra lithium in LVO on the capacitor with a 2:1 ratio. Cell voltage, positive, and negative electrode potentials are plotted against time in charge and discharge of an AC/LVO cell in 50 mA $g^{-1}$ and 3.5 V, but their prelithiation differs, ending at (a) 2.0 V and (b) 0.5 V (*vs.* $Li/Li^+$); respectively.

RSC Advances Accepted Manuscript

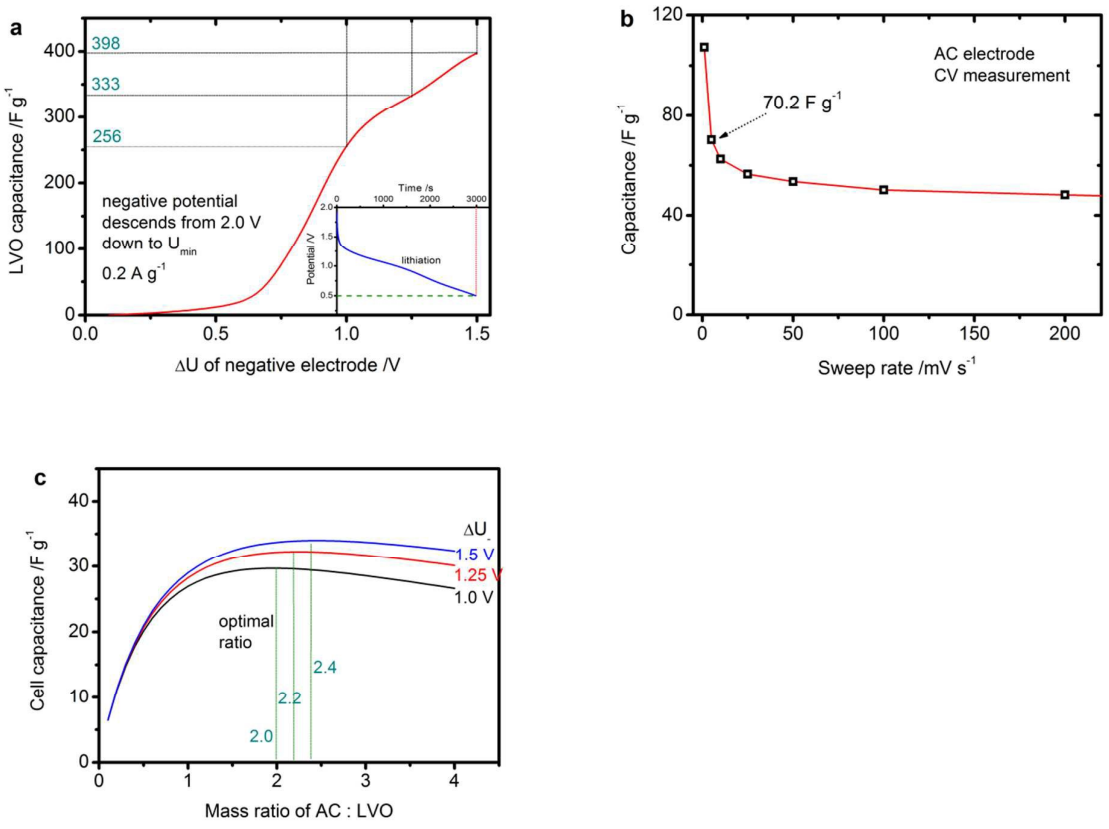


**Figure 5** Estimation of the optimal AC:LVO ratio. (a) LVO electrode capacitance in F $g^{-1}$ versus the potential difference of the negative electrode $\Delta U_-$ that starts at 2.0 V (*vs*. $Li/Li^+$). The inset shows the lithiation curve at 200 mA $g^{-1}$ of LVO electrode that this calculation is based on. (b) The AC capacitance being selected in calculating the optimal mass ratio. (c) Calculated values of the cell capacitance versus the AC:LVO mass ratio, based on Eq. (2).

RSC Advances Accepted Manuscript

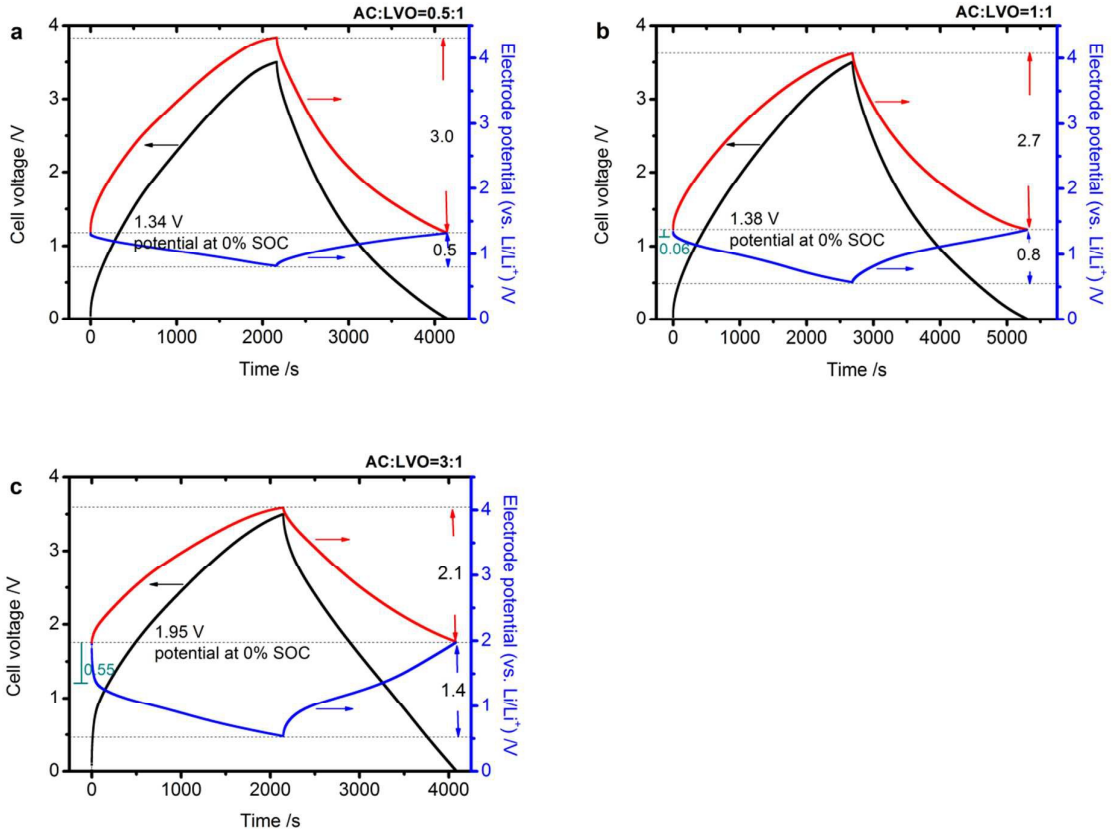


**Figure 6** Electrode potentials of the AC/LVO capacitors with three mass ratios. Cell voltage, positive and negative electrode potentials of the cell with AC:LVO= (a) 0.5:1; (b) 1:1; (c) 3:1 at 50 mA $g^{-1}$. Note the plot of the 2:1 cell has been shown in Figure 4b. Values of $\Delta U_+$ and $\Delta U_-$ are marked, along with $U_{0\%SOC}$.

RSC Advances Accepted Manuscript

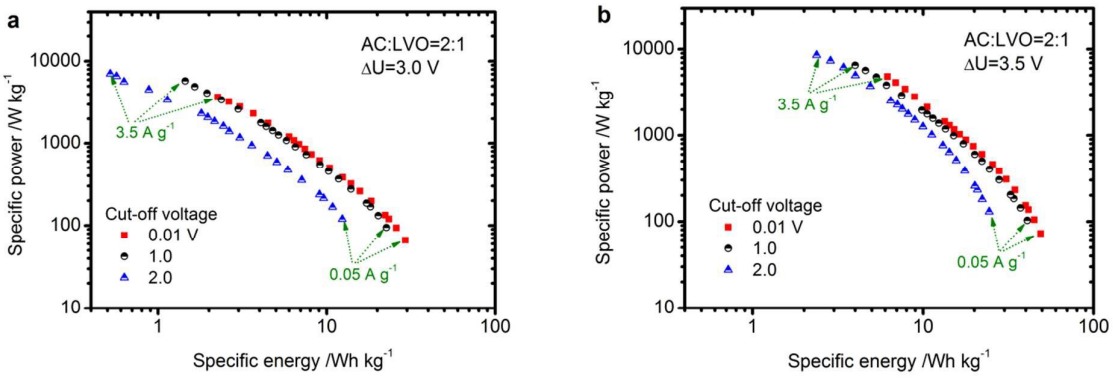


**Figure 7** Ragone plots of the AC/LVO capacitor with a 2:1 ratio. Specific energy values of the cell are plotted against specific power values, operated with (a) $\Delta U$=3.0 V and the cut-off voltage 0.01, 1.0, 2.0 V; (b) $\Delta U$=3.5 V and the cut-off voltage 0.01, 1.0, 2.0 V.

RSC Advances Accepted Manuscript

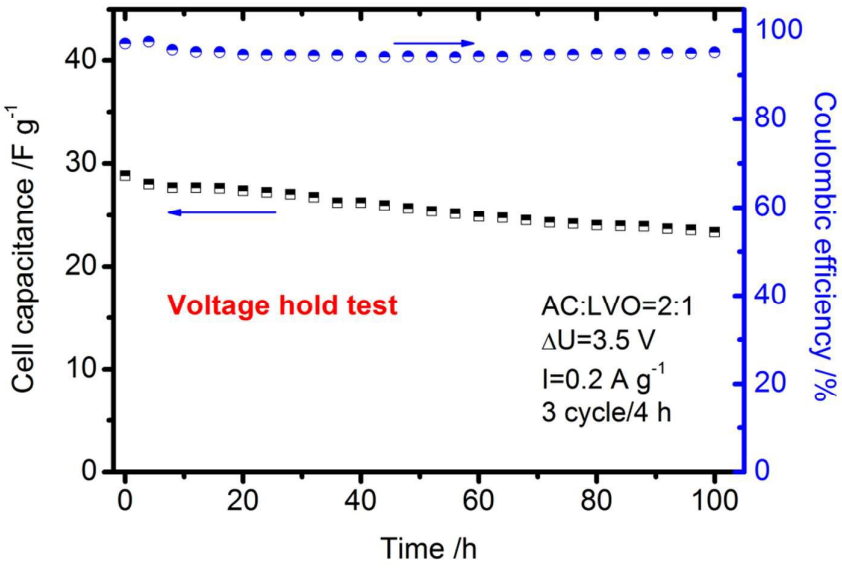


**Figure 8** Stability of the AC/LVO cell with 2:1 mass ratio. Variations of cell capacitance and coulombic efficiency during 100 h voltage hold in $\Delta U$=3.5 V.

RSC Advances Accepted Manuscript